Tomographic reconstruction of the ionosphere using ground-based GPS data in the Australian region

Endawoke Yizengaw[1], Peter Dyson[2], and Elizabeth Essex[3]

[1] Physics Department, La Trobe University, Bundoora, Vic 3086, Australia
E-mail: E.yizengaw@latrobe.edu.au

[2] As (1) above, but E- mail E-mail: P.dyson@latrobe.edu.au

[3]As (1) above, but E- mail: E.essex@latrobe.edu.au

ABSTRACT

This paper describes the experimental procedures of tomographic imaging techniques that have been developed and used at La Trobe University. Tomographic imaging provides a powerful technique for obtaining images of the ionospheric electron density distribution, and is a relatively new technique which has promising features to supplement the most expensive ground-based vertical sounding instruments such as ionosonde and incoherent radar. The technique, which involves monitoring radio transmission from Global Positioning System (GPS) along a meridional chain of ground based receivers, has particular potential for complementing temporal measurements by other observing techniques such as ionosondes. The tomographic inversion algorithm has been applied to actual GPS-based total electron content (TEC) measurements obtained during two severe magnetic storm periods (18 August 2003 and 31 March 2001). The tomographic reconstruction presented here revealed important features in ionospheric structure such as ionization troughs and quasi-wave formations. Electron density profiles obtained by the tomographic reconstruction method are in excellent agreement with profiles obtained by ionosondes at or near the GPS receiver stations, confirming the validity of the tomographic algorithm that has been developed. Geophysical interpretations of the observations are also presented.

Key words: Tomographic reconstruction, TEC, and GPS

INTRODUCTION

The knowledge of the electron density distribution in the Earth's ionosphere and plasmasphere is important for several purposes, such as: estimation and correction of propagation delays in the Global Positioning System (GPS); improving the accuracy of satellite navigation; predicting changes due to ionospheric storms; predicting space weather effects on telecommunications, and many more.

During the past decades, the scientific community has developed and used different observing instruments to gather information on the ionosphere and plasmasphere. Examples are vertical incidence sounders (ionosonde), incoherent scatter radars [1], topside sounders onboard satellites [2], in situ rocket and satellite observations [3], and occultation measurements [4]. Reception at the ground of signals from satellite radio beacons, such as GPS satellites, has become the most widely used method for investigations of ionospheric irregularities [3]. One of the advantages of this method is that, because of satellite motion, large segments of the ionosphere can be investigated in a comparatively short time interval and it is possible to observe variations in the satellite signals caused by irregularities of various dimensions. The time taken to record satellite signals for radio tomography can be as large as 25 minutes, however, in most cases (of course, not always) large ionospheric structures with dimensions of tens, hundreds and thousands of kilometres vary only slightly over such a period of time. Hence, using ground based GPS TEC measurements and radio tomography it is possible to observe important large-scale ionospheric features such as ionization troughs ([5], [6]), travelling ionospheric disturbances [7], boundary blobs, and other ionization irregularities that occur, for example, near the mid-latitude trough region [5].

Since Austen et al [8] first proposed the possibility of studying the ionosphere using satellite radio tomography, tomographic reconstruction of the ionospheric and plasmaspheric electron density has become a popular and successful means of studying the detailed features of the ionosphere and plasmasphere. Ionospheric studies using satellite radio

tomography offer several advantages over traditional ground-based instruments such as incoherent backscatter radars and ionosondes. Firstly, tomography is inexpensive: with the exception of the transmitting satellites, the cost of all equipment (primarily receiver, antenna and computers), is small compared to the cost of an incoherent backscatter radar or ionosonde. Suitable orbiting spacecraft, such as GPS, are provided for other purposes, eliminates the large expense of spacecraft construction and launch. Secondly, all the equipment for a single receiving site is readily transportable, allowing the investigation of ionospheric regions to be readily extended to regions not currently covered by other methods. A third advantage of radio tomography is its wide area of coverage at a given time interval as long as there are enough receivers across the region of interest, whereas other methods (mentioned above) do have a limited area of coverage as they are quite expensive to put them in networks around a limited area of coverage ([6], [9] and the references therein). However, if these instruments, regarded as other methods, are arranged in networks across a limited area of coverage, it is obvious that they will provide images of ionospheric electron density in reasonably less time than GPS tomography.

Furthermore, ground based radar measurements are restricted to either the bottomside ionosphere (ionosondes) or the lower part of the topside ionosphere (usually below about 800 km) so only the tomographic technique using satellites in high altitude orbits (e.g. GPS at ~20,000 km) is capable of providing details on the structure of the entire topside ionosphere and even of the plasmasphere above. In satellite radio tomography, now commonly referred to as Computerized Ionospheric Tomography (CIT), total electron content (TEC) measurements are inverted and reconstructed to obtain a two-dimensional electron density profile. The TEC, which is the main input to CIT, is defined as the integral of the electron density from the ground height up to the ceiling height, i.e., the height of the transmitting satellite (GPS satellite in our case). The electron density above approximately 2000 km provides only a small contribution (< 5%) to the TEC. The TEC measurement is obtained from observations of signal phase difference or of pulse travel time. In the case of GPS satellites, the TEC is usually derived from the time delay of the GPS signal. However, the total delay of a GPS signal as observed by a GPS receiver is due to several contributions. These are the dispersive ionospheric delay, the non-dispersive tropospheric delay, the non-dispersive apparent delays due to system clock errors, and the dispersive radio frequency delays in the radio frequency stages of the transmitters and receivers [3]. The determination of TEC from GPS observations involves the measurement of the differential group delay between the two frequencies as this eliminates the non-dispersive contributions to the delay time. Therefore only the dispersive terms are required to be considered for TEC calculation. The instrumental (receiver and transmitter) dispersive delay, known as instrumental biases, can be removed by appropriate calibration of the transmitters and receivers. There are different ways of then determining TEC from GPS differential group delay measurements, however, we have used a standard method described in [10].

This paper presents a new approach of ionospheric observation in the Southern Hemisphere: the reconstruction of the electron density distribution from ground based GPS TEC. It describes all the required input parameters to this reconstruction, the methods and procedures of the reconstruction experiment, and finally it presents tomographically reconstructed observation results for the Australian region. The independent verification of the reconstructed electron density is also presented.

EXPERIMENT

Satellites in the GPS system are orbiting our planet in 55° inclination at an altitude of 20200 km with an orbiting period of ~12 hr which corresponds to an angular velocity $\omega=0.0001456$ *rad/s*. The GPS satellites transmit signals at two coherent frequencies, namely at $L_1 = 1.57542$ *GHz* and $L_2 = 1.22760$ *GHz*. Hence, the tomographic network along the Australian Eastern region consists of a chain of five ground based GPS receivers with data acquisition systems as signal receivers. The geographic locations of the five receiving stations are, from south to north, Hobart (42.80°S, 147.44°E), Tidbinbilla (35.38°S, 148.97°E), Ceduna (31.87°S. 133.81°E), Alice Springs (23.67°S, 133.89°E), and Townsville (19.63°S, 146.85°S). As depicted in Fig.1, the geographic locations of the five stations span a range of 23.17° (from 19.63°S to 42.80°S) in latitude and all are within 9° of 140°E longitude. The ionosphere varies much more rapidly with latitude than longitude so we make the important assumption that longitudinal TEC gradients are relatively small and can be ignored. Thus all the TEC measurements recorded at the above GPS stations can be considered to provide information along the 140°E meridian. Hence, the local time difference between each GPS data point and the longitude of meridian, 140°E, can be eliminated by calculating the time difference due to their longitude differences. This can be mathematically given by:

$$LT_{140} = LT_{GPS} + \Delta UT \tag{1}$$

where LT_{140} is the local time at 140°E, LT_{GPS} is the local time at each GPS data points, and ΔUT is the local time difference between LT_{140} and LT_{GPS}. Thus the aim of the research reported here was to observe large-scale ionospheric structures over the Australian East coast region by applying tomographic imaging techniques, specifically designed at La Trobe University, to TEC measurements from the GPS satellites.

Reconstruction Methods

There are two basic types of reconstruction methods: algorithms using algebraic equation simulating methods (often called pixel based methods) and algorithms using a Fourier transform method (sometimes called non-pixel based methods) [11]. Reference [11], supported by results produced by these different methods, clearly presents the difference between these two reconstruction methods. For this study we used a pixel reconstruction method and thus, by assuming that the electron density distribution is unchanging during the satellite passes [12], the reconstruction plane is discretized into two-dimensional pixels as shown in Fig.1.

Usually, but not necessarily, the grid of these two dimensional boxes is subdivided equidistantly with height and angular spacing. For the present study the grid boxes are 10 km in height and 1° (~100 km) in width as shown in Fig.1. By assuming that the electron density is constant in each pixel, the TEC along the ray path can be represented as a finite sum of shorter integrals along segments of the ray path length. Mathematically this can be expressed as:

$$\boldsymbol{STEC}_i = \sum_{j=1}^{M} n_j d_{ij} + e_j \tag{2}$$

or, generally in a simple matrix notation (referred below),

$$\boldsymbol{Y}_{T\times 1} = \boldsymbol{D}_{T\times M}\ \boldsymbol{N}_{M\times 1} + \boldsymbol{E}_{T\times 1}\,. \tag{3}$$

where $\boldsymbol{Y}$ is a column of T measurements, $\boldsymbol{N}$ is a column of the M unknown n_js, $\boldsymbol{E}$ is a column of T values representing the error due to data noise and discretization, $\boldsymbol{D}$ is a $T \times M$ matrix with d_{ij} being the length of link i that lies in pixel j, and thus d_{ij} is 1 if the i^{th} ray traverses through the j^{th} pixel and 0 otherwise. The error element of $\boldsymbol{E}$ has two components: the measurement noise and the error introduced by discretization. Given the high precision of TEC measurements obtainable with the GPS system, the error in $\boldsymbol{E}$ is dominated by the latter of these two errors. The discretization error will be a function of the size of the pixel and the variability of the medium. Hence, (3) can be simplified as:

$$\boldsymbol{Y}_{T\times 1} = \boldsymbol{D}_{T\times M}\ \boldsymbol{N}_{M\times 1}\,. \tag{4}$$

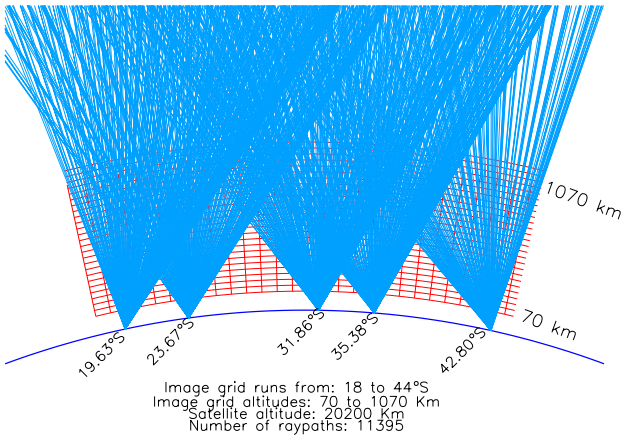

Fig.1. The experimental setup showing the GPS satellite ray paths recorded for durations of 20 minutes at the five GPS receivers at latitudes indicated. Only one tenth of the rays are shown for clarity. Note that most of the rays are close to vertical, and none of the rays is horizontal. As a consequence some of the pixels making up the full image space are not intersected by the GPS ray paths, and this is the basic difficulty of ionospheric tomography that uses ground based GPS receivers alone.

However, an inversion algorithm is required to determine the unknown electron density distribution from known $\boldsymbol{Y}$ and $\boldsymbol{D}$. So many different inversion techniques have been developed since Austen and his team [8] first announced CIT as a potentially suitable technique for ionospheric research. Reference [14] reviewed CIT reconstruction algorithms proposed by various investigators. One of the most commonly used inversion techniques is called algebraic reconstruction technique (ART). The ART algorithm, which can converge quickly in an iterative fashion compared to other reconstruction algorithms, is the preferable algorithm to use for ionospheric reconstruction in a region of interest with a limited widely spaced number of receivers, like the GPS receiver network in the Australian region. Due to these preferences, the ART algorithm has been used in this paper. However, it usually suffers from the effects of noise, which can be caused by inconsistencies introduced in the set of equations, and it is possible to reduce this noise by introducing an appropriate relaxation parameter (mentioned below) as shown in (5). Basically, the ART algorithm, which requires an initial guess to start with, improves the reconstruction on the initial guess with the collected experimental TEC data in an iterative fashion and can be implemented as the following equation describes:

$$\boldsymbol{N}^{k+1} = \boldsymbol{N}^{k} + \lambda_k \frac{STEC_i - \sum_{j=1}^{M} d_{ij} n_j^k}{\sum_{j=1}^{M} d_{ij} d_{ij}} \boldsymbol{D}_i \qquad (5)$$

where $\boldsymbol{D}_i$ is the i^{th} row of $\boldsymbol{D}$, k is iteration number, and λ_k is the relaxation parameter. The relaxation parameter ensures that the correction remains stable, and it is a real number usually confined to the interval $0 < \lambda_k < 2$. The value of λ_k is usually chosen to be the same for all iterations. In our case $\lambda_k = 0.005$ has been used for all iterations. This relaxation parameter value was chosen from experience in which the author identified the best λ_k value where the solution converges quickly with a reasonable number of iterations. For our case the root mean square (RMS) difference was used to compare the actual data and the model slice (noise) after the convergence of ART algorithm, and an average magnitude of 0.0015 TECU has been found during severe magnetic storm observation (31 March 2001). During magnetically quiet period this magnitude of noise has even reduced to ~ 0.00089 TECU. These minimum RMS values confirm the assumption of error elimination which is mentioned above.

Background information

As mentioned above, the ART algorithm requires some initial values of the quantity to be reconstructed. This initialization can represent a gross estimate or a guess of what the reconstruction might look like; the first iteration of the reconstruction algorithm will begin to correct this guess toward some satisfactory solution. Several different approaches to the reconstruction have been proposed. For this paper we used the combination of two models, IRI-2001 and Chapman profile models, to produce vertical electron density profiles at 1° interval of latitude. By adopting the peak height information obtained from nearby ionosonde stations, we have generated different Chapman and IRI-2001 model density profiles at different times of the day. The IRI-2001 model profile shows evidence for a nighttime E-layer electron density enhancement peak at about 110 km altitude or thereabout. Of course the IRI-2001 model requires further optional input parameters such as f_oF_2 and $M(3000)F_2$ to get a reasonably true density profile, which sometimes includes the nighttime E-layer. The above mentioned further input parameters can be obtained from ionosonde measurement data. However, the possibility of the E-layer ionization was not included in the range of vertical profiles calculated from Chapman method. On the other hand, the Chapman profile has a better density profile for the topside ionosphere than the IRI-2001 model, which is very thick above the F2 peak. Therefore, to benefit from the information of these two profiles, the described topside information, from Chapman profile, are now attached to the subset of bottom side profiles, which is obtained from IRI-2001 model, to produce a new set of background profiles at intervals of 1° in latitude. Thus, the new set of backgrounds that we used to start our tomographic algorithm can be represented in matrix form as $I_{H \times S}$ for H height and S latitudinal pixels.

OBSERVATIONS

Tomographic reconstructions of real GPS TEC data, obtained by the method described above, have been performed for the ionosphere in the Australian region. Ground based GPS TECs are selected for reconstruction based upon two criteria. The first is that the elevation of the satellite at each receiving station should be greater than 20°. The reconstruction algorithm includes facilities to automatically reject GPS data of elevation angle less than 20°, even if the

ray paths intersect the image plane. The second criterion is the number of ray paths that cross the image plane. To ensure a reasonable number, GPS data from at least four receiver stations are required. Tomographic reconstruction campaign have been conducted for data that have been recorded from September 1999 to August 2003. When we say data from September 1999 to August 2003, it doesn't mean that the entire four year data have been reconstructed but the majority of the data, especially during magnetically active periods, have been reconstructed. Because tomographic reconstruction for data during quite periods in the mid-latitude ionosphere was almost quite smooth and can't demonstrate the capability of the ionospheric tomography experiment that we developed. Therefore, to clearly demonstrate the performance of our tomographic reconstruction experiment, here we present the observation data that have been obtained during two severely active geomagnetic periods, 18 August 2003 and 31 March 2001. The geomagnetic activity during these days was extreme and three-hourly Kp values through the first period were 6-, 6+, 7, 7-, 7, 7+, 6+, 6, and through the second, 7-, 9-, 9-, 6+, 7, 8, 8+, 7+.

Among other radio tomography results (mentioned in section 1), the most interesting structure detected in the ionosphere is the ionization trough which is a daytime and nighttime feature of the ionosphere. The nighttime ionization trough has been well studied by different means of observations [5], [15]. However, the mid-latitude trough has been less frequently observed on the dayside of the Earth's ionosphere. Reference [6], which described the NNSS radio tomography experiment, has reported observations of the ionization trough on the dayside of the Earth's ionosphere at high latitudes, which were verified by observations with EISCAT. They also observed an apparent equatorward movement of the daytime trough, which is the well established behaviour of the nighttime trough.

Fig. 2 shows examples of typical tomographic images of the dayside ionosphere obtained during the magnetically active period on August 18, 2003. A height-versus-geographic latitude grid has been used. The first panel (Fig. 2a), obtained from data recorded at 02:00-02:25 UT (11:30-11:55 LT), shows a clear density trough at ~35.0°S. Further south, the density increased, reaching a peak at 38.0°S latitude. It then reduced, forming a shallow minimum near 42.0°S latitude before again increasing slightly. However, to the north of the trough, the density remained uniform. The second panel (Fig. 2b), obtained using data recorded at 03:30-03:55 UT (13:00-13:30 LT), again shows a well pronounced trough, this time with a minimum at 32.0°S. The density distribution to the north and south of the trough are now essentially the same with a value in excess of $17.0 \times 10^5\ cm^{-3}$. The earlier ionization bay observed at 42.0°S latitude (see first panel) is now fully disappeared and the mid-latitude density distribution become uniform with latitude.

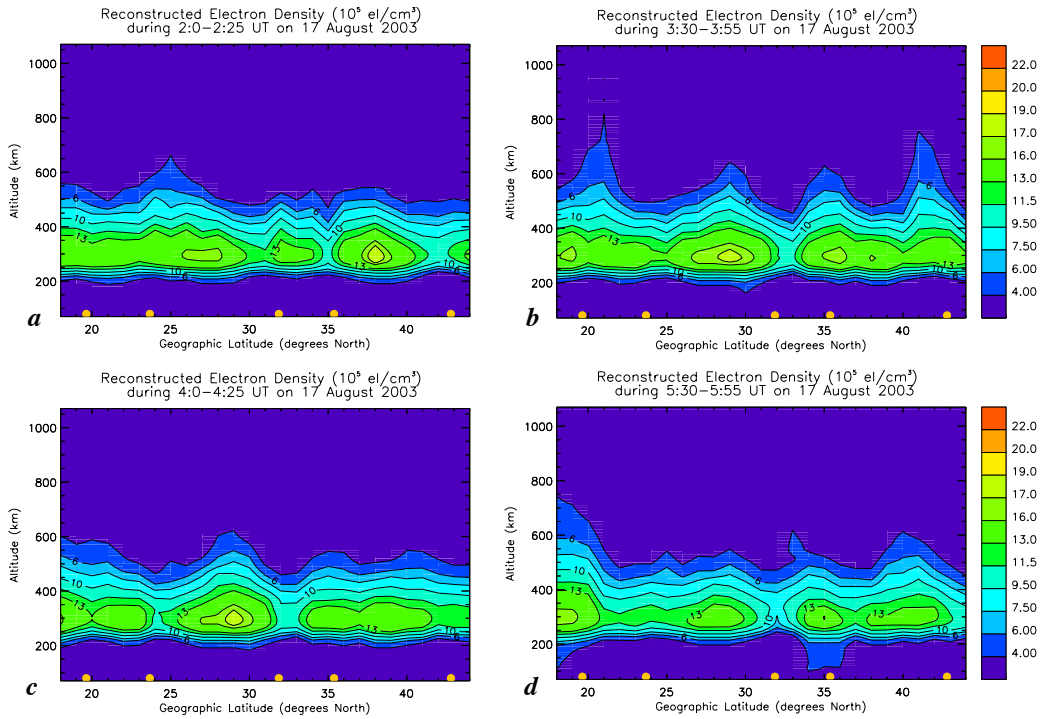

Fig. 2a-d. Tomographic images monitored on 18 August 2003 derived from GPS data in the Australian region. The recording time intervals for each panel are given at the top of each panel.

A similar well pronounced trough, with a minimum at 32.0°S, is evident in the third panel (Fig. 2c), derived from data recorded at 04:00-04:25 UT (13:30-13:55 LT). The peak densities to the north again exceed $17.0 \times 10^5\ cm^{-3}$, however, the F-region density values to the south are now slightly reduced and reached a maximum value of only $14.0 \times 10^5\ cm^{-3}$. The last panel (Fig. 2d), for 05:30-05:55 UT (14:00-14:25 LT) time period, also revealed a rather wide trough with a trough minimum at 32.0°S latitude. The peak density distributions to the north and south of the trough minimum are equal with a value of $14.0 \times 10^5\ cm^{-3}$. Here there is evidence of an enhanced E-layer density between 34.0°S and 36.0°S latitudes.

The trough shown in the first panel is rather narrow in comparison with that in the fourth panel. In the latter case the trough has considerable depth compared to the earlier troughs. The densities in this latter image are slightly less than those of the troughs at earlier times with the peak density being only $8.0 \times 10^5\ cm^{-3}$ at the trough minimum, compared to a peak density of $11.0 \times 10^5\ cm^{-3}$ at the trough minimum in Fig. 2a. There has also been an apparent equatorward movement of the trough minimum, from latitude of 35.0°S to 32.0°S, during the 210 minutes separating the two plots. The reconstruction images in the missing panels (between 02:00 UT and 03:30 UT) have also revealed this feature.

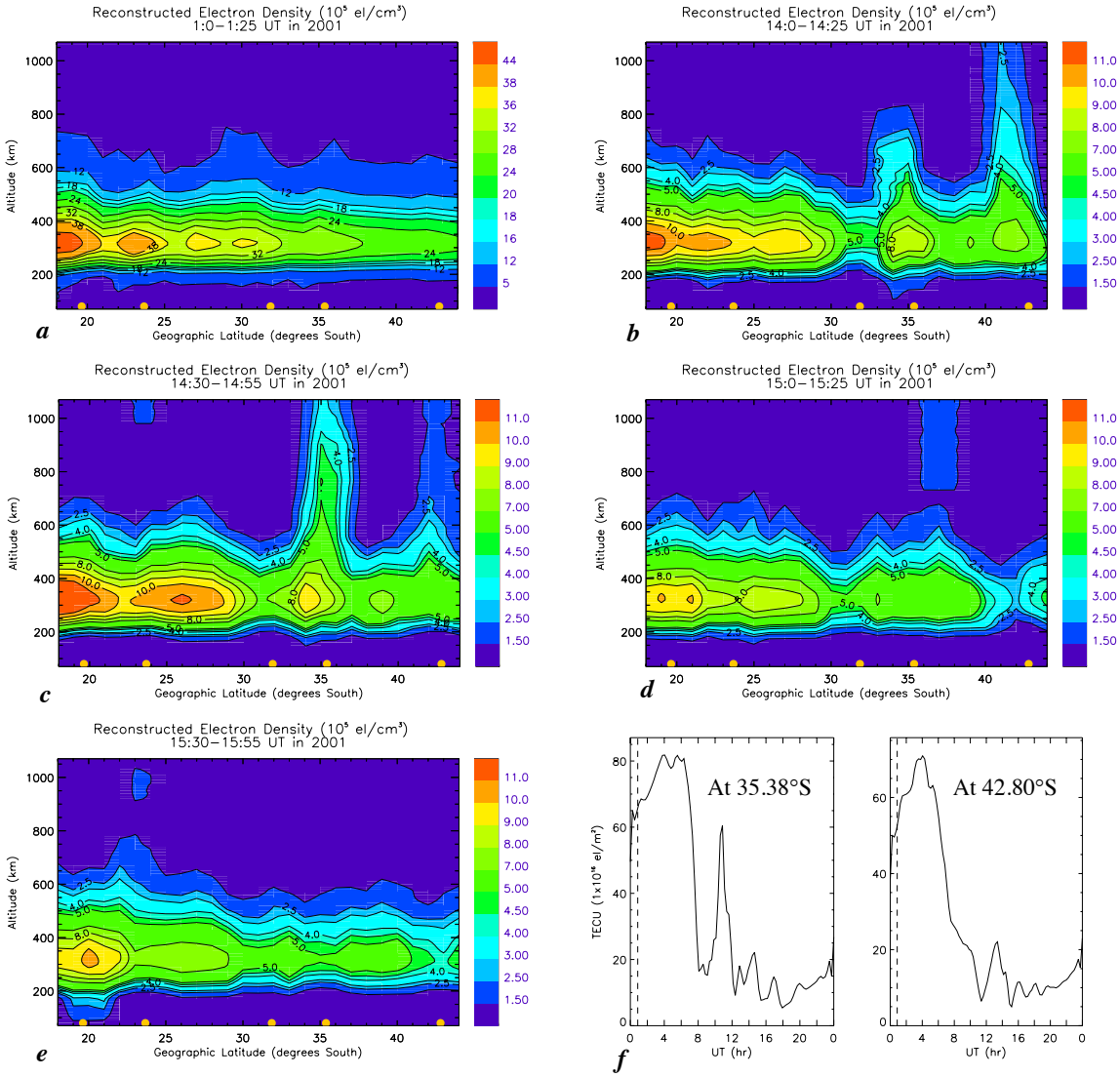

Fig 3a-e. Tomographic reconstructions for ground-based GPS TEC data recorded, at the five stations in the Australian region, on 31 March 2001, and 3f is the vertical TEC recorded at 35.38°S and 42.80°S latitude stations.

Tomographic reconstruction can also readily detect the details of other structures in the ionosphere. This includes various wave and quasi-wave structures that perturb the ionosphere, demonstrating that tomography can be an important technique for studying some types of ionospheric irregularities. The tomographic images derived from ground based GPS TEC during an equinoctial geomagnetically active period (31 March 2001) are shown in Fig. 3. The density distribution displayed in the first panel, for the period 01:30-01:55 UT (10:00-10:25 LT), shows the normal, solar-produced ionization maximum at the lower latitudes, with the maximum densities decreasing to the south. Attention shall be given to the scale and contour interval difference between the daytime (Fig. 3a) and nighttime (Fig. 3b-e) countour maps. The average F-layer peak density height is about 325 km. On the contrary the nighttime tomographic images shown in the second and third panels (Fig. 3b and 3c), for the same day, reveal unusual kind of ionospheric structure. Long finger-like formations with a height (of 400-500 km or even greater) and with a width of 300-400 km are presented in second and third panels of Fig. 3. The intensity of these finger-like ionization features is different at different locations. For examples, an intense electron density appeared first at higher latitude centred at 41.0°S, and then within 30 minutes it migrated to lower latitudes leaving the signature of a weak density at its previous position, as shown in Fig. 3b and 3c. In the fourth panel (Fig. 3d), for 15:00-15:25 UT (00:30-00:55 LT) time period, the initial position of the feature is displaced with an ionization trough like structure with a maximum density of $2.5 \times 10^5\, cm^{-3}$ in the vicinity of the trough. Despite that the second position of the peak density feature, which was centred at 35.0°S in Fig. 3c, acquired a weak density feature in Fig. 3d compared to its earlier density features that are shown in the second and third panels. There has been an evidence from the tomographic reconstruction image presented in Fig. 3e that this finger-like density feature was further migrated to even lower latitudes, resulting in a comparatively narrow (50-100 km) finger-like structure at lower latitude centred at ~23.5°S. Fig. 3e also revealed that the finger-like density feature at any of its previous positions has no any symptom of existence. The density distribution in the vicinity of the trough like structure, which was centred at 41.0°S in Fig. 3d, is now recovered and reached a value in excess of $4.5 \times 10^5\, cm^{-3}$. This indicates that the density distribution is returning to its normal density distribution trend after the period of intense magnetic activity.

DISCUSSION AND CONCLUSION

The tomographic data from the disturbed geomagnetic period revealed a persistent dayside trough in the vicinity of the return flow of the dusk convection cell. The electric potential pattern, from the Defense Meteorological Satellite Program (DMSP) ionospheric convection model (not shown here), for IMF value (at about 05:00 UT) of the disturbed period (18 August 2003) clearly indicates that the negative electric potential, which is an indication of the convection flow, extended down to the south coast Australian region during the time of local afternoon. Here the region of sunward return flow of the dusk convection cell, which may, as suggested by [16], be bringing plasma that has been circulating in darkness into the higher density region of the dayside ionization. Reference [16] suggested that the trough was in the region of return sunward flow where depleted plasma from the nightside was displacing dayside ionization. Although this phenomenon is a well defined feature of subauroral latitude regions, during severe magnetic storm periods it expands further down to lower latitude regions [15]. The tomographic reconstruction result, shown in Fig. 2, then revealed the equatorward migration of the trough from about 35.0°S to 32.0°S. This could be due to an abrupt increase in magnitude of the interplanetary magnetic field (IMF), when B_y changed from -16.3 nT at 0000 UT to 9.9 nT at 0200 UT and B_z from 6.2 nT at 0000 UT to -15.4 nT at 0200 UT. The values of B_y and B_z remained quite strongly positive and negative, respectively, until ~ 0600 UT. This led to a dramatic change in plasma structuring. The tomographic observation during this period showed that the ionosphere responded to the event with a marked equatorward displacement of the trough minimum (referred above), which is again in keeping with the observations of [15] and [16].

The finger like structures of the ionosphere that have been observed during the severe magnetic storm on 31 March 2001 required careful analysis to be established as real ionospheric structures. To answer the question of whether or not these structures are the artefacts of the algorithms used in the tomographic reconstruction, it is important to note the vertical TEC values across the density features. Thus, Fig 3f depicts the vertical TEC at positions near the finger-like formations, i.e., at 35.38°S and 42.80°S. In both cases they indicate an ionization enhancement across the locations of the finger-like formations. Hence, from the point of view of all the characteristics of the formation, such as its movement to lower latitudes and displacement of peak electron density as the electron density decreases (Fig. 3b and 3d), the correlation of the formation with the wave disturbance of the ionosphere is visible, and in this case the fingers are tails of the crests and the depletion of ionization is the trough of the wave disturbances. The appearance of quasi wave structures when the ionosphere is in a perturbed state, more significantly during the periods when $K_p > 4$, has been well studied with the help of different observation techniques ([6], [7]). Similar finger-like structures have been observed previously with the help of incoherent scattering radars [1] and of course with the help of the tomographic reconstruction method [7].

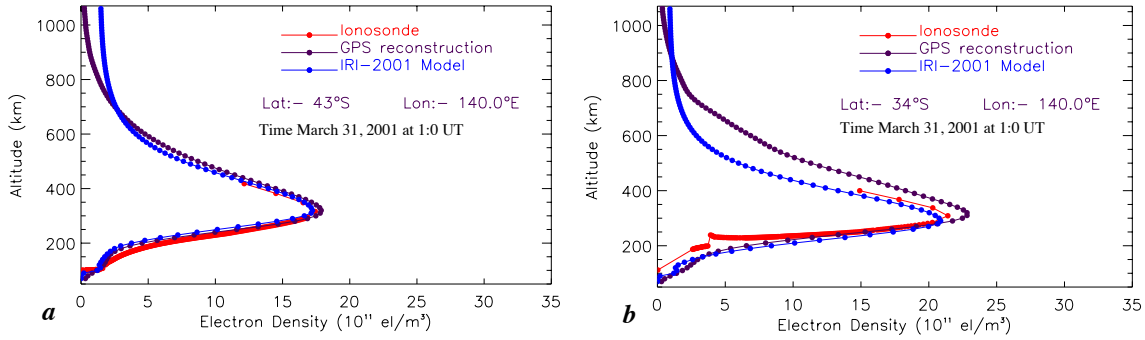

Fig. 4a-b. The tomographically reconstructed electron density profiles (black dots) are verified with the corresponding density profile (red dots) measured by ionosonde stations located at (a) Hobart and (b) Canberra. Comparison with IRI-2001 density profiles (blue dots) is also presented.

The available ionosonde stations in the Australian region provided independent comparisons to the tomographically obtained electron density profiles. Fig. 4 provides verification of the typical output of radiotomography, for 01:00-01:25 UT (10:30-10:55 LT) time period on 31 March 2001, with the available valid ionosonde data recorded at nearby stations to the GPS receiving sites and with density profiles from IRI-2001 model. In Fig. 4a the vertical profile at 43°S has been plotted, showing that tomographically reconstructed density profile has agreed with ionosonde data from Hobart and IRI-2001 model. Fig. 4b depicts that the profile at 34°S again agreed quite well with those independently measured data and model profiles, except around the peak, where the reconstruction appeared to yield slightly higher densities than the ionosonde data and IRI-2001 model. However, the H_{max} of both profiles is the same, and there is good agreement at the bottom side densities, but less for the topside, which could be probably due to the scale height selection error for the topside Chapman profiles. Despite that the types of features of the ionosphere (discussed above) are not represented by empirical models, like IRI-2001 model, which are mainly representing monthly average data (usually based on ionosonde measurements). Although such average models are very useful for giving guidelines for monthly averages of behaviour and show diurnal variations well, they can not reproduced short lived (minutes to hours) events that occur sporadically. Needless to say these short lived events of the ionosphere may affect the normal time density distributions. It is of fairly certain interest to note that our inversion method can catch these short-lived features, showing fair density profile agreement with a similar ionosonde data recorded independently at nearby stations. For some reason the ionosonde at Canberra did not catch up the bottom side density distribution properly, especially density profiles below 250 km height, where substantial data gap are pronounced.

In conclusion excellent agreement between these independently measured data and our extensive reconstruction density profiles, as shown in the typical examples in Fig. 4a&b, confirms the capability of ionospheric tomography in detecting the different important features of the ionosphere. Even high resolution density profiles can be achieved when the inversion technique use more assorted data from quite dense ground-based GPS receivers (< 2° separation between two neighbouring receivers) across the region of interest and if data is also supplemented from space based GPS receivers, which can provide horizontal crossing slant TEC. In that case tomography will therefore be a good replacement to ground based vertically sounding instruments, mentioned above, because tomographic reconstruction technique is a much less expensive technique than radar and ionosonde instruments.

ACKNOWLEDGMENT

This work has been supported by the La Trobe University Postgraduate Scholarship scheme and Cooperative Research Center for Satellite Systems (CRCSS) top-up scholarship. Thanks are due to Dr. P. Wilkinson and staffs of IPS Radio and Space Services for providing the Ionosonde data, Geoscience Australia National Mapping Division (formerly Australian Surveying and Land Information Group (AUSLIG)) and IGS for the GPS data.

REFERENCES

[1] R.T. Tsunoda, "High-latitude F-region irregularities: a review and synthesis," *Rev. Geophy*., Vol. 26, pp. 719-760, 1988.

[2] B.W. Reinishch, D.M. Haines, R.F. Benson, J.L. Green, G.S. Sales, and W.W.L. Taylor, "Radio sounding in space: Magnetosphere and topside ionosphere, " *J. Atmos. Sol. Terr. Phys.,* vol. 63, pp. 87-98, 2001.

[3] J.A. Klobuchar, "Ionospheric effects on GPS," *GPS World*, April, pp. 48-51, 1991.

[4] N. Jakowski, A. Wehrenpfennig, S. Heise, Ch. Reigber, H. Lühr, L. Grunwaldt, and T.K. Meehan, "GPS radio occultation measurements of the ionosphere from CHAMP: Early results," *Geophys. Res. Lett.*, vol. 29, pp. 95-1-95-4, 2002.

[5] L. Kersley, J.A.T. Heaton, S.E. Pryse, and T.D. Raymund, "Experimental ionospheric tomography with ionosonde input and EISCAT verification," *Ann. Geophysicae*, vol. 11, pp. 1064-1074, 1993.

[6] S.E. Pryse, L. Kersley, M.J. Williams, and I.K. Walker, "The spatial structure of the dayside ionospheric trough," *Ann. Geophysicae*, vol. 16, pp. 1169-1179, 1998.

[7] V.E. Kunitsyn, E.D. Tereshchenko, E.S. Andreeva, B.Z. Khudukon, and Y.A. Melnichenko, "Radiotomographic investigation of ionospheric structures at auroral and middle latitudes," *Ann. Geophysicae*, vol. 13, pp. 1242-1253, 1995.

[8] J. R. Austen, S. J. Franke, and C. H. Liu, "Application of computerized tomography techniques to ionospheric research," in *Radio Beacon contributions to the study of ionization and dynamics of the ionosphere and to corrections to geodesy and technical workshop*, A. Tauriainen, Eds. pp. 25-35, Ouluensis Universitas, Oulu, Finland, 1986.

[9] C.N. Mitchell, L. Kersley, J. A. T. Heaton, S. E. Pryse, "Determination of the vertical electron-density profile in ionospheric tomography: experimental results," *Ann. Geophysicae*, vol. 15, pp. 747-752, 1997.

[10] Breed, A.M, 1996. Investigation of the ionosphere over Australia using satellite transmissions. Ph.D. thesis, School of Applied Physics, University of South Australia.

[11] E. Sutton and H. Na, "Static Tomographic Reconstruction of the Time Varying Ionosphere," *IEEE Signal Processing Society*, IEEE Computer Society Press. 1996.

[12] L.C. Tsai, C.H. Liu, W.H. Tsai, and C.T. Liu, "Tomographic imaging of the ionosphere using the GPS/MET and NNSS data," *J. Atmos. Sol. Terr. Phys.* Vol. 64, pp. 2003-2011, 2002.

[13] V.E. Kunitsyn, E.S. Andreeva, and O.G. Razinkov, "Possibilities of the near-space environment radio tomography," *Radio Sci.*, vol. 32, pp. 1953-1963, 1997.

[14] T.D. Raymund, "Ionospheric tomography algorithms," *Int. J. Imaging Sys. Tec.*, vol. 5, pp. 75-85, 1994.

[15] M. Mallis and E. A. Essex, "Diurnal and seasonal variability of the southern-hemisphere main ionospheric trough from differential- phase measurements," *J. Atmos. Terr. Phys.*, vol. 55, pp. 1021-1037, 1993.

[16] J. A. Whalen, "The daytime F layer trough and its relation to ionospheric-magnetospheric convection," *J. Geophys. Res.*, vol. 94, pp. 17169-17184, 1989.